Supporting Information

An "electronegative" bifunctional coating layer: simultaneous regulation of polysulfide and Li-ion adsorption sites for long-cycling and "dendrite-free" Li–S batteries

Qian Lu [a], Xiaohong Zou [a], Ran Ran [a], Wei Zhou [a], Kaiming Liao [a, *] and Zongping Shao [a, b]

[a] State Key Laboratory of Materials-Oriented Chemical Engineering, College of Chemical Engineering, Nanjing Tech University, Nanjing 210009, China
[b] WA School of Mines: Minerals, Energy and Chemical Engineering (WASM-MECE), Curtin University, Perth, WA 6845, Australia

Q.L. and X.Z. contributed equally to this work.

* Corresponding author, E-mail: kaimingliao@njtech.edu.cn

Supplementary Figures and Tables

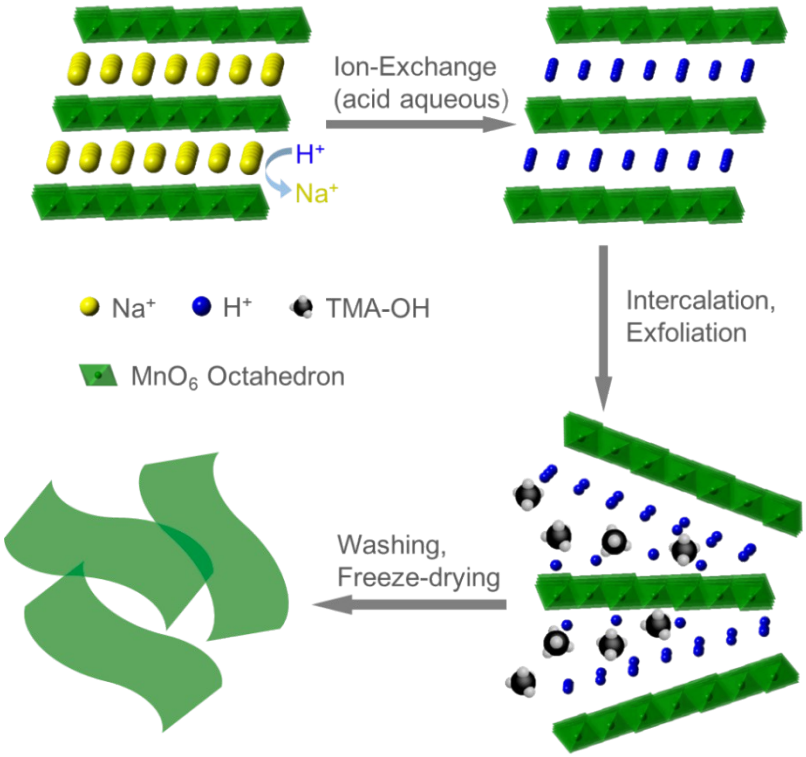

Figure S1. Schematic illustration of synthetic procedures of the H_xMnO_{2+x} nanosheets.

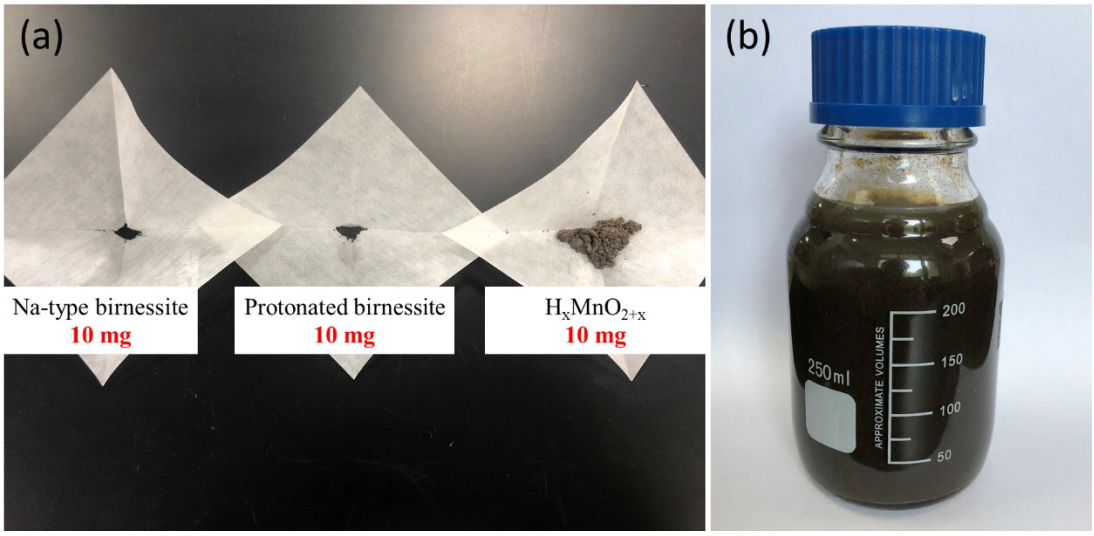

Figure S2. Photographs of (a) Na-type birnessite, protonated birnessite, and delaminated H_xMnO_{2+x} powder with the same mass; (b) delaminated H_xMnO_{2+x} suspension in TMAOH solution.

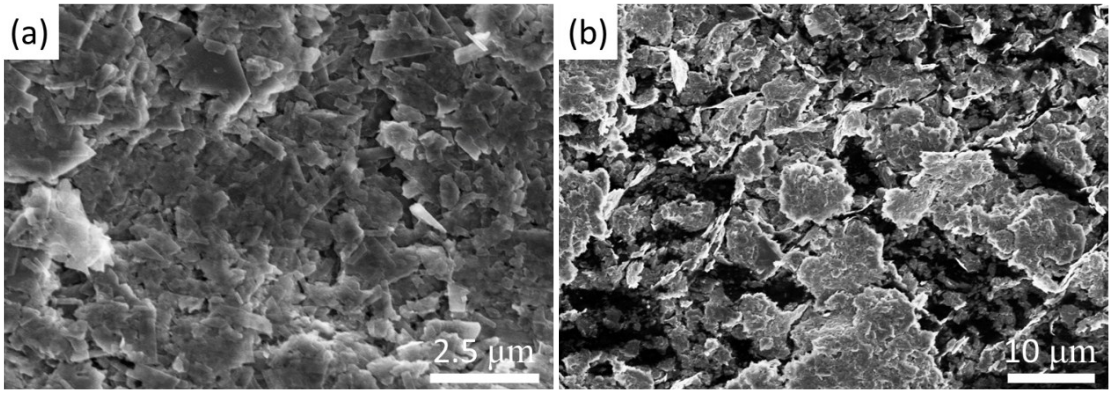

Figure S3. SEM images of Na-type birnessite.

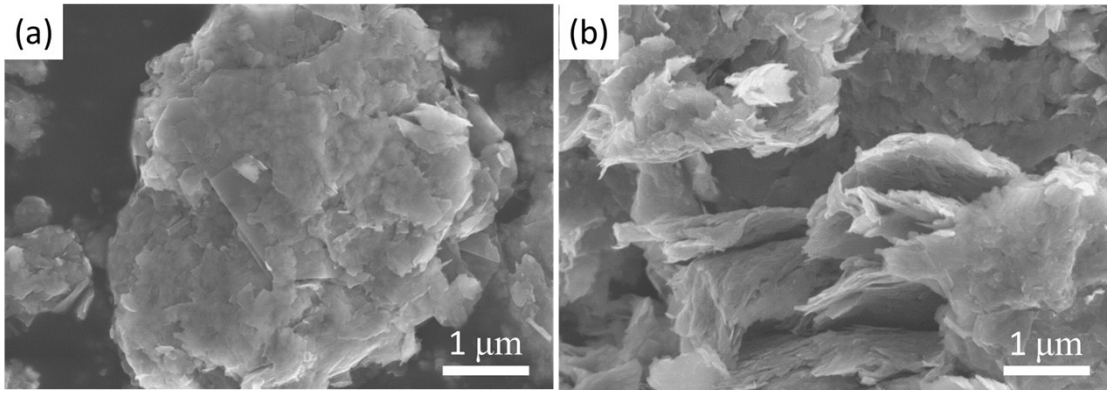

Figure S4. SEM images of protonic birnessite.

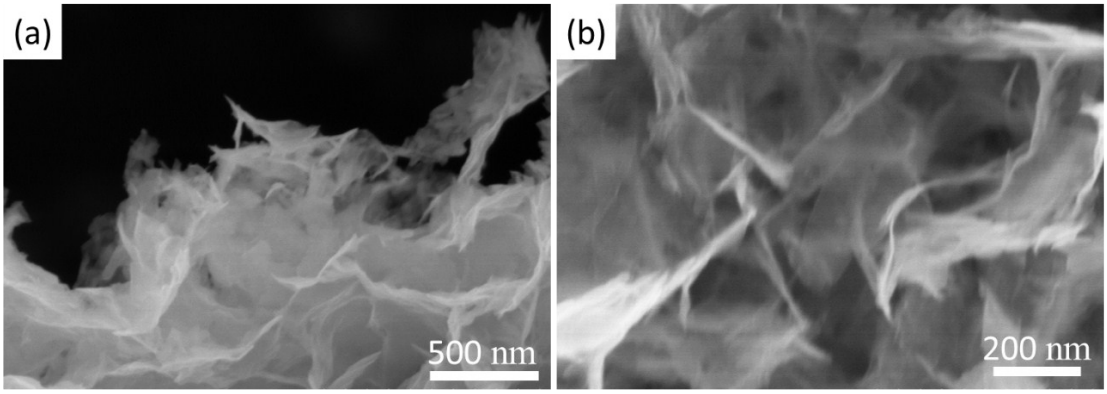

Figure S5. SEM images of delaminated H_xMnO_{2+x} nanosheets.

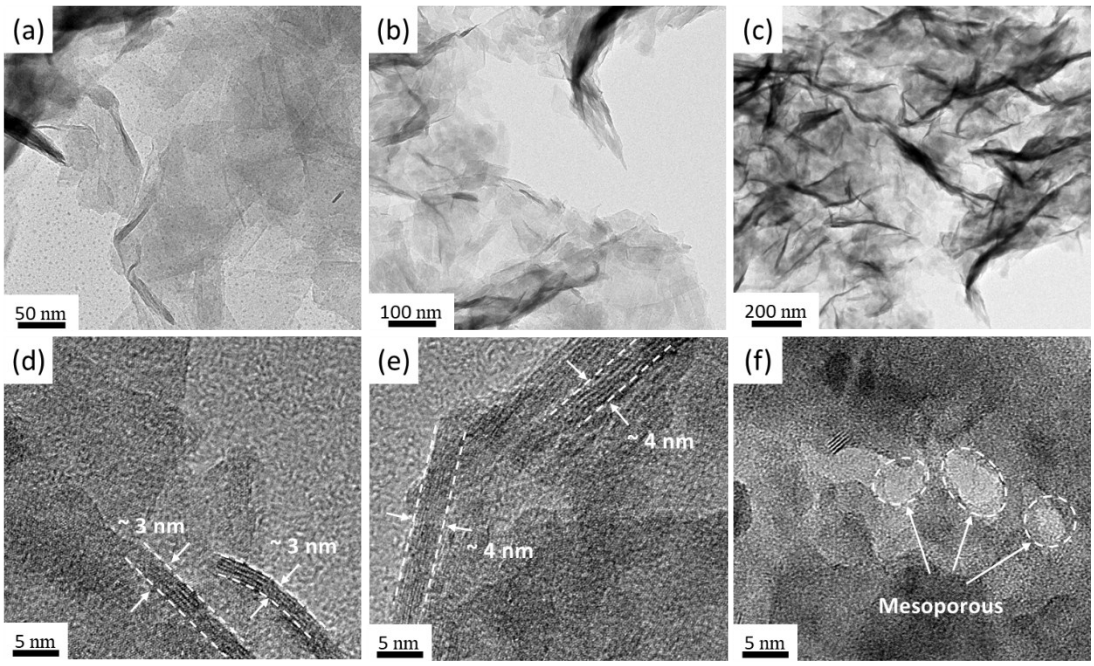

Figure S6. (a, b, c) TEM image and (d, e, f) HRTEM image of delaminated H_xMnO_{2+x} nanosheets.

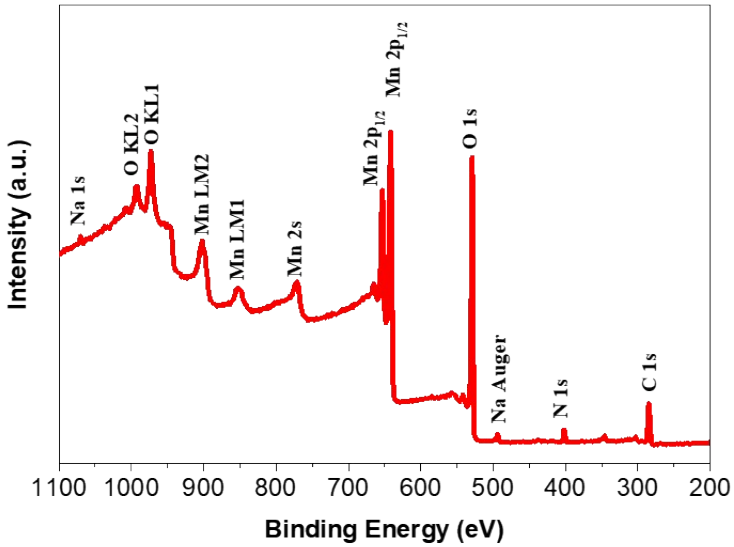

Figure S7. XPS survey of delaminated H_xMnO_{2+x} nanosheets.

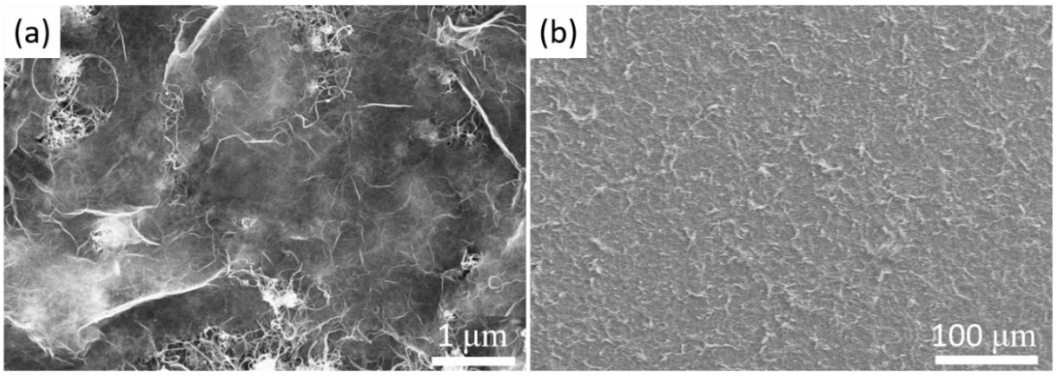

Figure S8. SEM images of G-PP separator from top view.

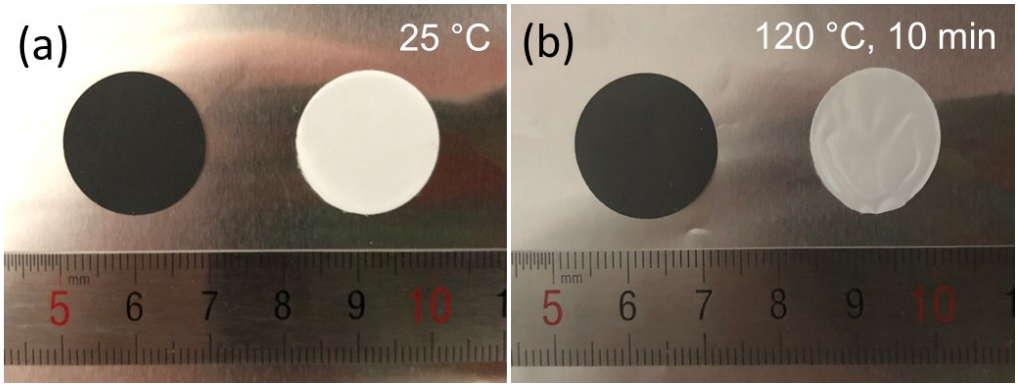

Figure S9. Digital photographs of the EB-PP (left) and PP (right) separator at heating temperature (a) 25 °C and (b) 120 °C.

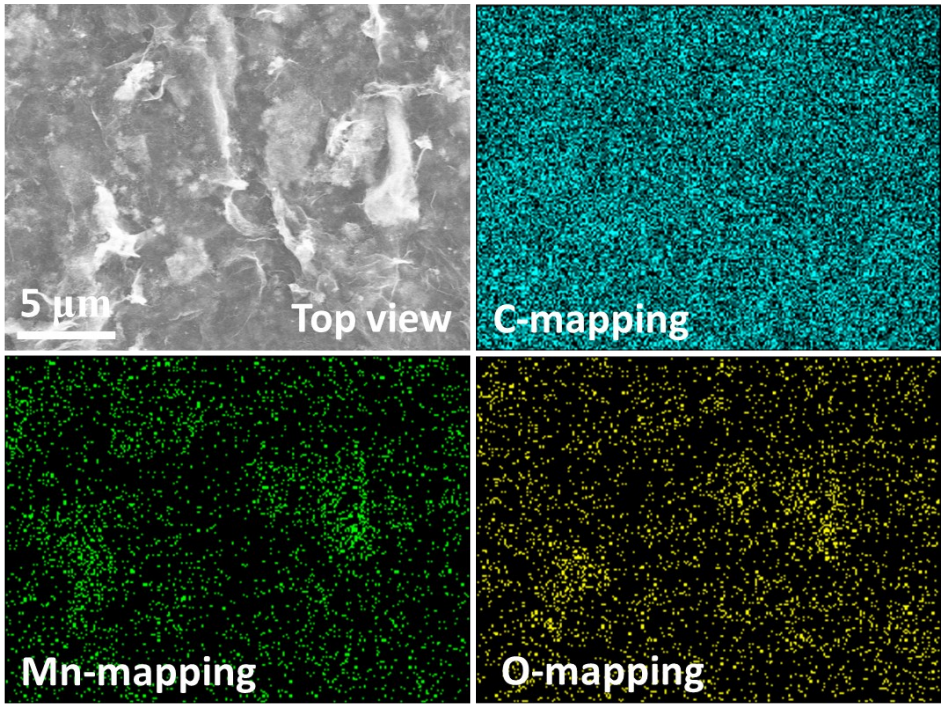

Figure S10. SEM images of EB-PP separator from top view and corresponding EDX mapping of C, Mn and O elements.

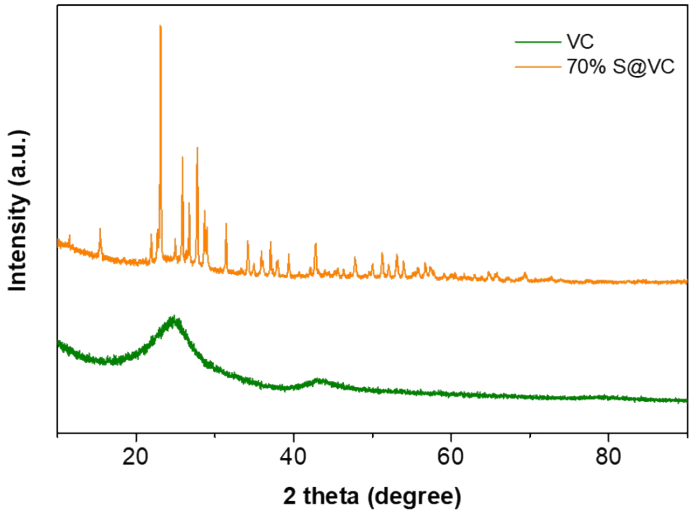

Figure S11. X-ray diffraction (XRD) patterns of Vulcan XC-72 and 70%S@VC.

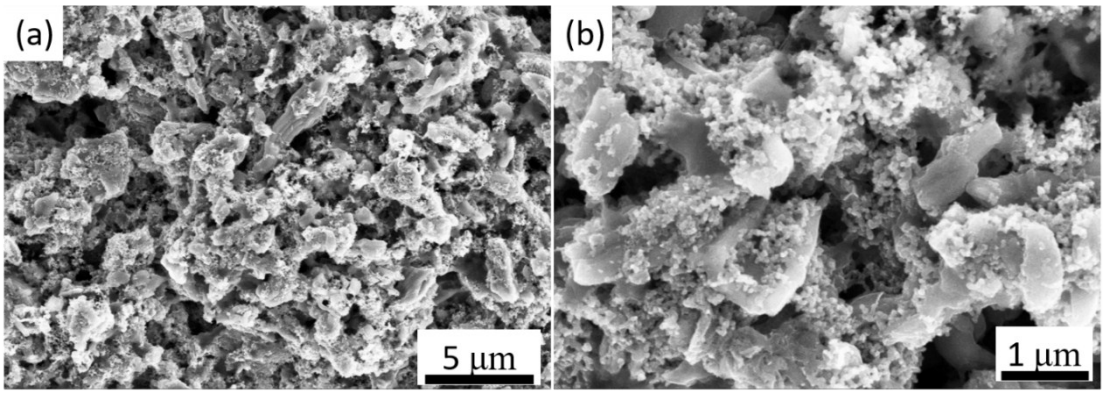

Figure S12. Surface SEM images of 70%S@VC cathode.

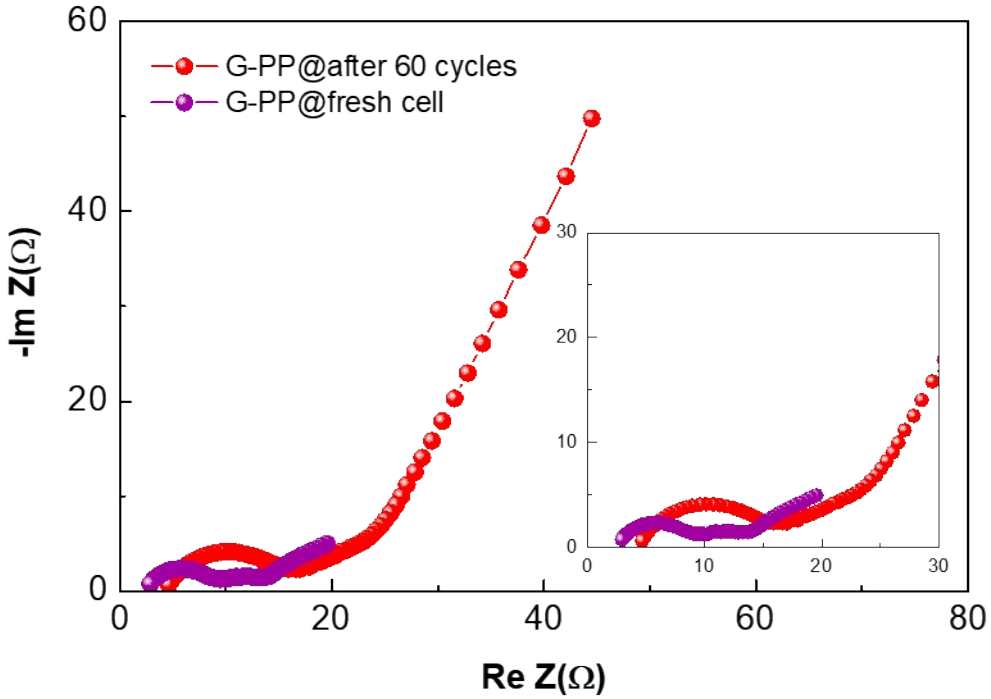

Figure S13. Electrochemical impedance spectra with G-PP separator collected before and after cycling, respectively

Table S1. The parameters gained from the EIS curves in Figure 4a.

Samples	First cycle R_e (Ω)	After 60th R_e (Ω)	First cycle R_{ct} (Ω)	After 60th R_{ct} (Ω)	First cycle R_f (Ω)	After 60th R_f (Ω)
PP	1.67	2.35	17.61	24.45	16.41	15.69
G-PP	2.56	4.33	5.50	10.41	6.34	13.69
EB-PP	1.55	2.16	18.17	15.61	\	\

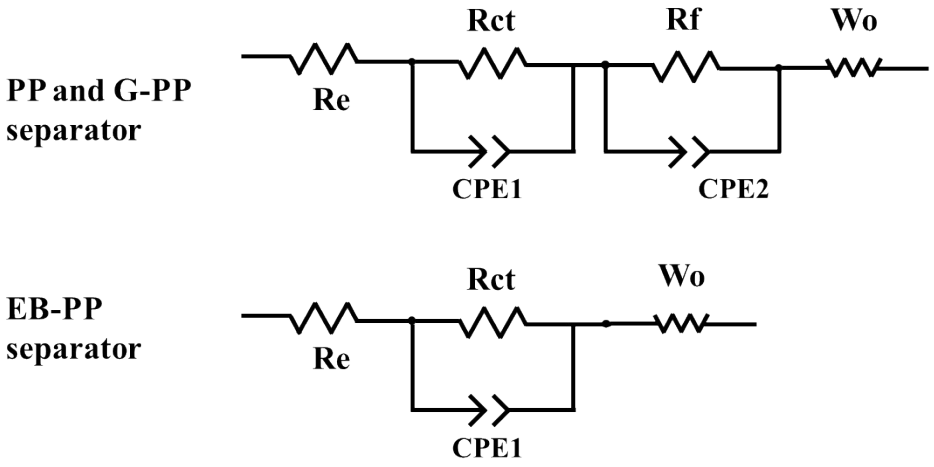

Figure S14. The equivalent circuit for PP, G-PP and EB-PP separator.

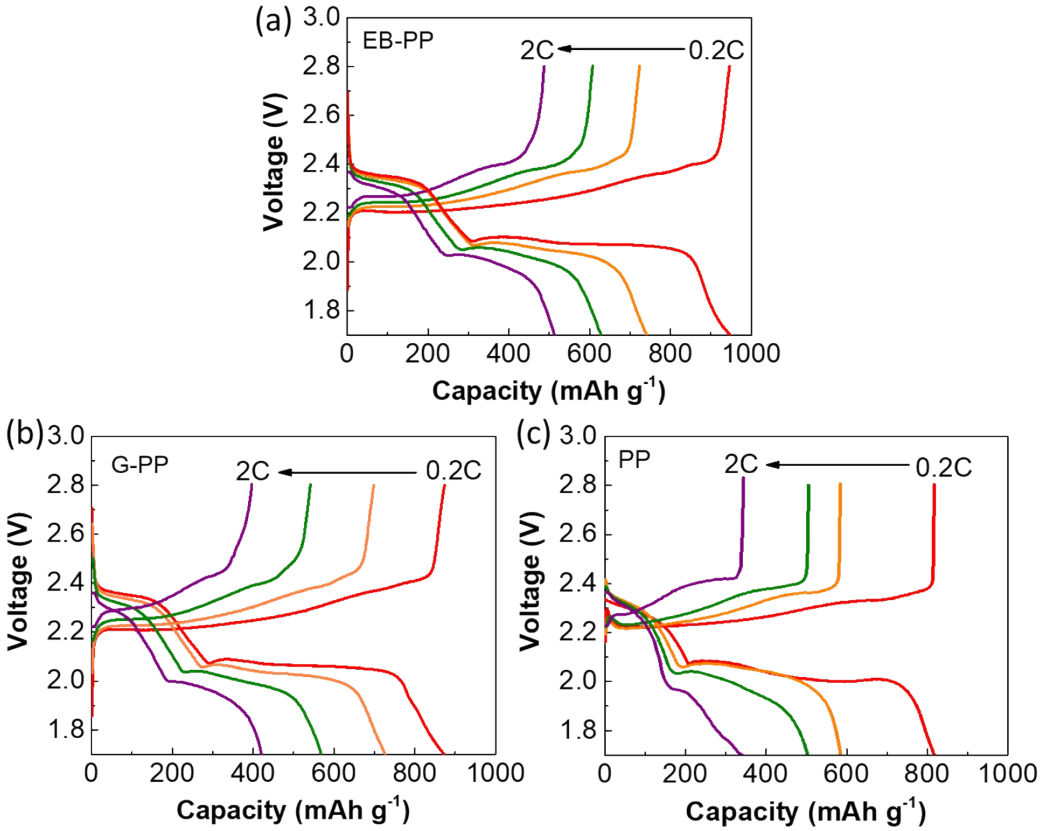

Figure S15. Charge-discharge curves of (a) EB-PP, (b) G-PP and (c) PP separators at various current densities from 0.2 to 2 C.

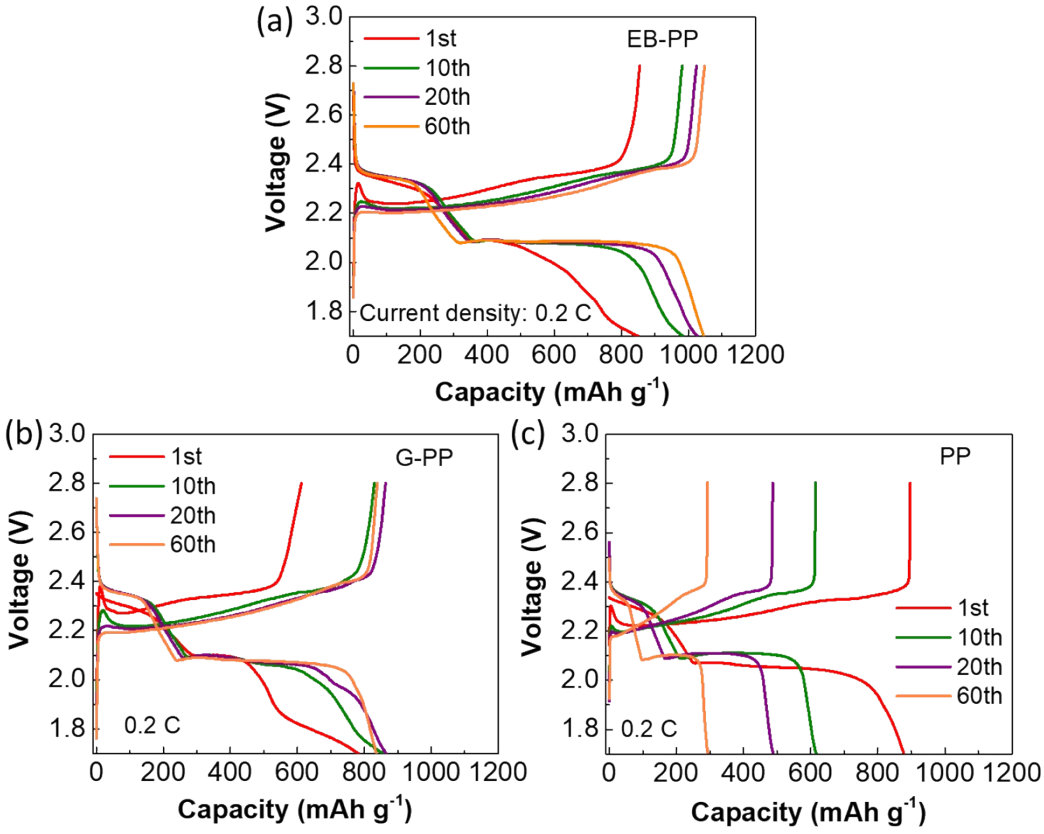

Figure S16. Charge-discharge curves of (a) EB-PP, (b) G-PP and (c) PP separators at various cycles at 0.2 C.

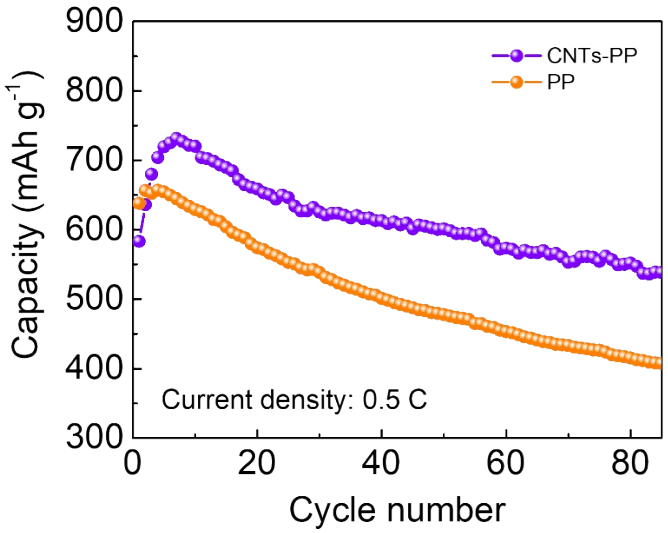

Figure S17. Cycling performance of Li-S battery with CNTs-PP and PP separator with sulfur mass load of 1.8 mg cm^{-2} at current density of 0.5 C.

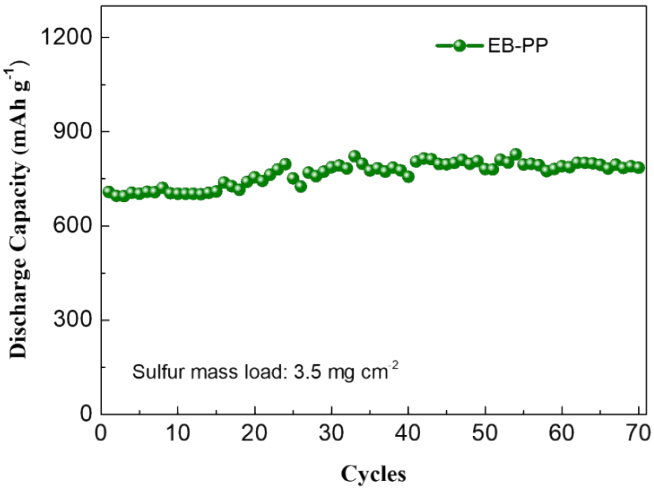

Figure S18. Cycling performance of Li-S battery with the EB-PP separator with sulfur mass load of 3.5 mg cm^{-2} at current density of 0.1 C.

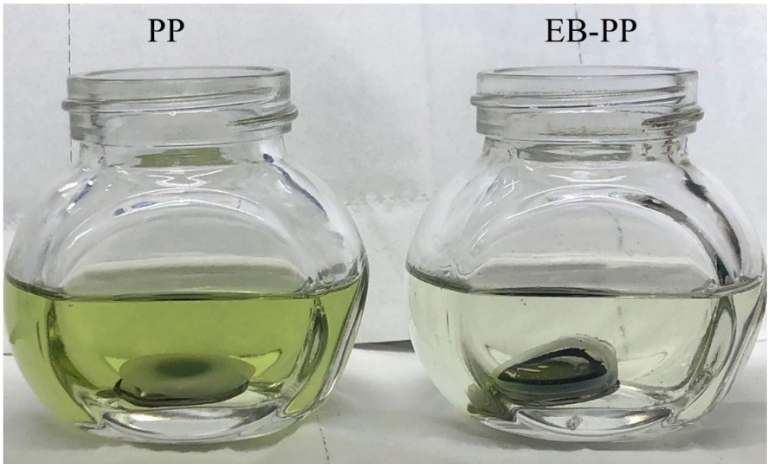

Figure S19. Immersing of the cycled electrode and separator harvested from the batteries with PP and EB-PP in DME solvent for 1 h.

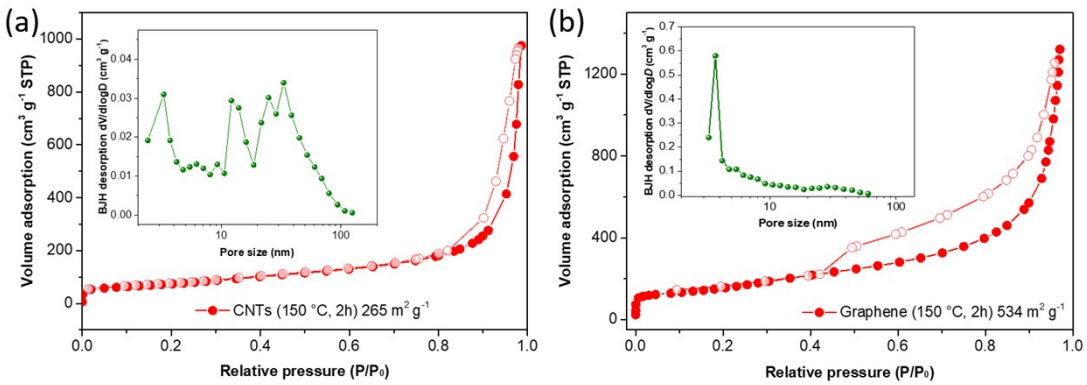

Figure S20. Adsorption/desorption isotherms and corresponding pore size distribution of (a) CNTs and (b) graphene.

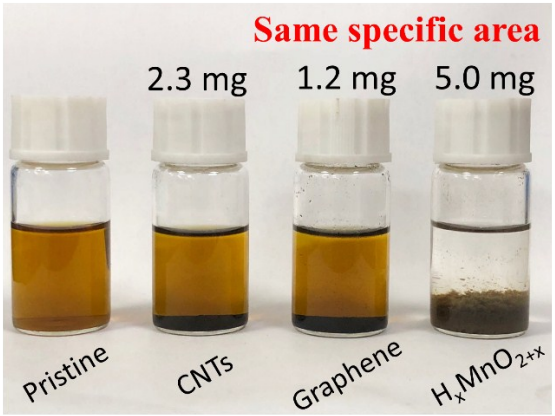

Figure S21. Sealed vials of the Li_2S_6 solution after contact with same specific area of different sample powders.

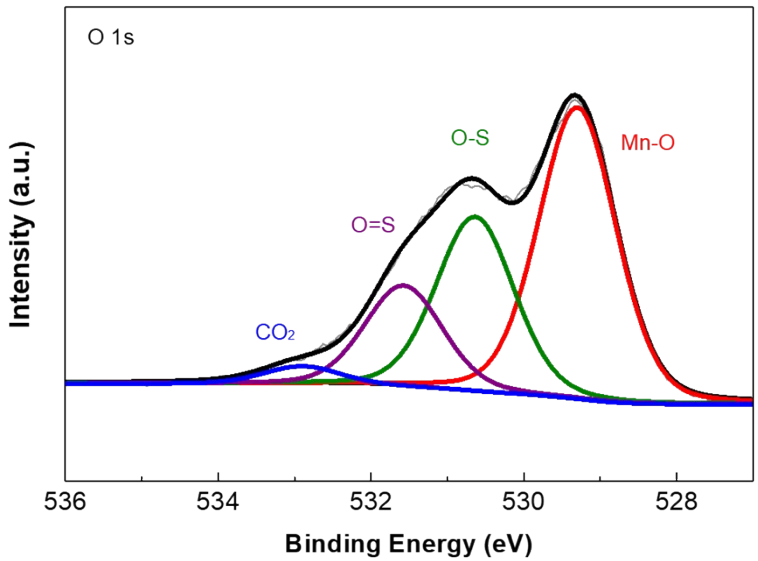

Figure S22. O 1s XPS spectra of H_xMnO_{2+x}@Li_2S_6.

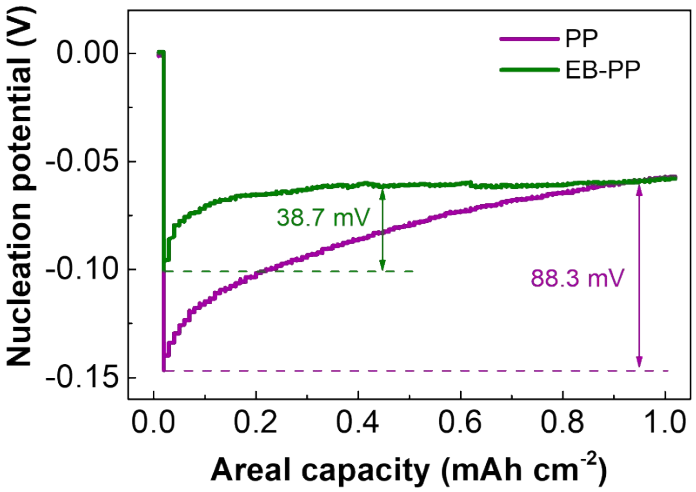

Figure S23. Nucleation overpotential of the Li symmetrical cells with PP seporator (purple line) and EB-PP seporator (green line).

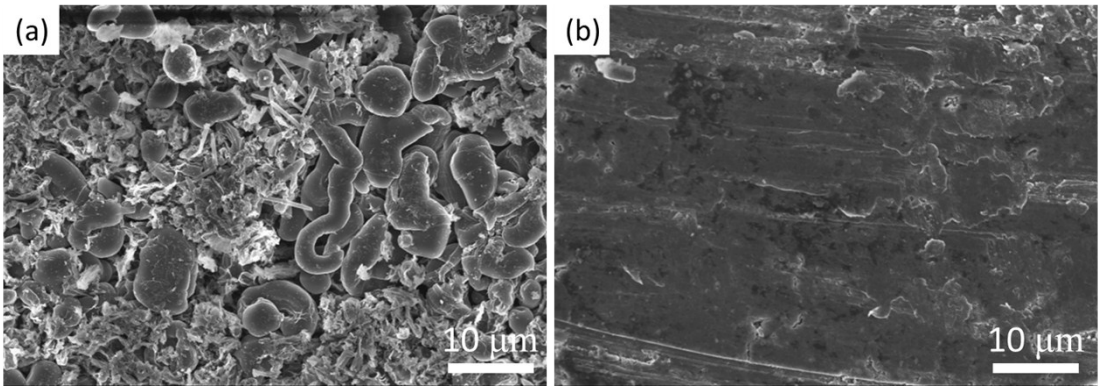

Figure S24. Surface SEM images of lithium anode with (e) PP seporator, and (f) EB-PP seporator after cycling.

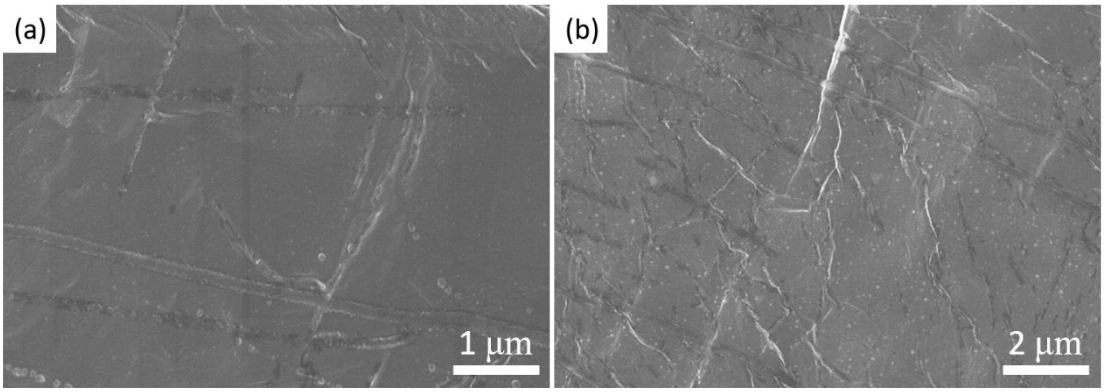

Figure S25. SEM images of fresh lithium metal.

Table S2. The performance of the Li-S batteries with various modified separators.

Barrier	**Weight of barrier** (mg cm^{-2})	**Thickness of barrier** (μm)	S loading (mg cm^{-2})	S content (wt%)[a]	**S content** (wt%)[b]	Current density (A g^{-1})[c]	**Capacity decay Cycles**	Ref
Graphene	1.3	30	1.5-2.1	70	38~43	1.5	0.064% 500 cycles	[S1]
Graphene oxide (GO)	0.29	0.75	1-1.2	60	47-48	1.67	~0.150% 400 cycles	[S2]
Mesoporous carbon	0.5	27	1.55	49	37	0.74	0.081% 500 cycles	[S3]
$Li_4Ti_5O_{12}$/ graphene	0.35	35	1.2	60	47	0.5	0.066% 300 cycles	[S4]
LDH/ graphene	0.3	2	1.1-1.3	63	50-51	3.2	0.060% 1000 cycles	[S5]
Ti_3C_2	0.4	2	0.7-1	48	31-34	0.84	0.262% 200 cycles	[S6]
SnO_2/rGO	0.15	20	2.87	55	52	1.67	~0.133% 200 cycles	[S7]
Fe_3O_4@ Graphene	0.478	30	0.6-0.9	60	33-39	1.67	0.024% 500 cycles	[S8]
MoO_3@CNT	0.577	30	1	60	38	0.5	0.190% 200 cycles	[S9]
$Li_6La_3Ta_{1.5}Y_{0.5}O_{12}$/Graphene	0.8	~11	1.8	60	42	0.84	0.095% 200 cycles	[S10]
TiO_2@carbon nanofibers	1.6	30	3	49	32	0.34	0.126% 300 cycles	[S11]
CNT@TiO_2	0.7	12	1.7	60	43	1.67	0.056% 1000 cycles	[S12]
B-rGO	0.2-0.3	25	1.45-1.56	56	46-50	0.167	0.1532% 300 cycles	[S13]
This work [d]	0.2	3	1.8	56	51	1.67	0.040% 1000 cycles	/

(a) the S contents of the sulfur composite cathodes, (b) the S contents of the sulfur composite cathodes after decorated with the barrier modified separator, (c) 1.67 A g^{-1} = 1 C, (d) EB-PP.

Reference

[S1] G. Zhou, L. Li, D. Wang, X. Shan, S. Pei, F. Li and H. Cheng, *Adv. Mater.*, 2015, **27**, 641-647.

[S2] M. Shaibani, A. Akbari, P. Sheath, C. Easton, P. Banerjee, K. Konstas, A. Fakhfouri, M. Barghamadi, M. Musameh, A. Best, T. Ruther, P. Mahon, M. Hill, A. Hollenkamp and M. Majumder, *ACS Nano*, 2016, **10**, 7768-7779.

[S3] J. Balach, T. Jaumann, M. Klose, S. Oswald, J. Eckert and G. Lars, *Adv. Funct. Mater.*, 2015, **25**, 5285–5291.

[S4] Y. Zhao, M. Liu, W. Lv, Y.-B. He, C. Wang, Q. Yun, B. Li, F. Kang and Q.-H. Yang, *Nano Energy*, 2016, **30**, 1-8.

[S5] H. Peng, Z. Zhang, J. Huang, G. Zhang, J. Xie, W. Xu, J. Shi, X. Chen, X. Cheng and Q. Zhang, *Adv. Mater.*, 2016, **28**, 9551-9558.

[S6] Y. Dong, S. Zheng, J. Qin, X. Zhao, H. Shi, X. Wang, J. Chen and Z. Wu, *ACS Nano*, 2018, **12**, 2381-2388.

[S7] N. Hu, X. Lv, Y. Dai, L. Fan, D. Xiong and X. Li, *ACS Appl. Mater. Interfaces*, 2018, **10**, 18665-18674.

[S8] Y. Liu, X. Qin, S. Zhang, G. Liang, F. Kang, G. Chen and B. Li, *ACS Appl. Mater. Interfaces*, 2018, **10**, 26264-26273.

[S9] L. Luo, X. Qin, J. Wu, G. Liang, Q. Li, M. Liu, F. Kang, G. Chen and B. Li, *J. Mater. Chem. A*, 2018, **6**, 8612–8619.

[S10] P. Kim, S. Narayanan, J. Xue, V. Thangadurai and V. Pol, *ACS Appl. Energy Mater.*, 2018, **1**, 3733−3741.

[S11] T. Zhao, Y. Ye, C. Lao, G. Divitini, P. Coxon, X. Peng, X. He, H. Kim, K. Xi, C. Ducati, R. Chen, Y. Liu, S. Ramakrishna and R.V. Kumar, *Small*, 2017, **13**, 1700357.

[S12] L. Yang, G. Li, X. Jiang, T. Zhang, H. Lin and J. Lee, *J. Mater. Chem. A*, 2017, **5**, 12506–12512.

[S13] F. Wu, J. Qian, R. Chen, Y. Ye, Z. Sun, Y. Xing and L. Li, *J. Mater. Chem. A*, 2016, **4**, 17033–17041.